VIPERLAB

FULLY CONNECTED **VI**RTUAL AND **P**HYSICAL **PER**OVSKITE PHOTOVOLTAICS **LAB**

D7.4 Update to D7.1, taking into account new device stacks, refined materials properties and optimized modelling

DELIVERABLE REPORT

Version: 1.2

Date: 04.12.2024

FULLY CONNECTED VIRTUAL AND PHYSICAL PEROVSKITE PHOTOVOLTAICS LAB VIPERLAB

DELIVERABLE

D 7.4 UPDATE TO D7.1, TAKING INTO ACCOUNT NEW DEVICE STACKS, REFINED MATERIALS PROPERTIES AND OPTIMIZED MODELLING

Project References

Project Acronym	VIPERLAB
Project Title	Fully connected **vi**rtual and physical **per**ovskite photovoltaics **lab**
Project Coordinator	Helmholtz-Zentrum Berlin
Project Start and Duration	1st June 2021, 42 months

Deliverable References

Deliverable No	D7.4
Type	Report
Dissemination level	Public
Work Package	WP7
Lead beneficiary	EPFL
Due date of deliverable	30-Nov-2024
Actual submission date	04-Dec-2024

Document history

Version	Status	Date	Beneficiary	Author
1.0	Draft	20.11.2024	EPFL	A. Hessler /C. Wolff
1.1	Revised	03.12.2024	EPFL	C. Wolff
1.2	Edited	04.12.2024	HZB	N. Maticiuc

DISCLAIMER

‘Fully connected virtual and physical perovskite photovoltaics lab' VIPERLAB is a Collaborative Project funded by the European Commission under Horizon 2020. Contract: 101006715, Start date of Contract: 01/06/2021; Duration: 42 months.

TABLE OF CONTENT

This project has received funding from the European Union's Horizon 2020 research and innovation programme under grant agreement N°101006715

EXECUTIVE SUMMARY

In the VIPERLAB project WP7, titled "JRA1-Materials and Device Innovation Infrastructure," aims to enhance data and knowledge sharing among the perovskite PV research community to address the rapid advancements in experimental progress. The objectives of this initiative include providing up-to-date insights through meta-studies, evaluating modelling tools and material libraries, and correlating simulation outputs with experimental data to identify key factors impacting device performance. As part of this effort, Task JRA1.2 “Analysis of available device modelling tools” focuses on analysing available device modelling tools, offering a detailed overview of optical and optoelectronic simulation solutions. By comparing these tools through round-robin studies and extracting meaningful parameters from simulations, the task accelerates research by identifying critical material properties and guiding processing improvements.

Report D7.4 is an update of the confidential report D7.1 which outlined simulation guidelines for improving the optical and electrical performance of perovskite and perovskite-silicon tandem solar cells within the VIPERLAB consortium. It describes three rounds of comparative simulations that examined various tools to identify their strengths, limitations, and differences. The findings of D7.1 emphasized the importance of critical parameters such as material properties, layer thicknesses, and doping levels in achieving optimal device efficiency.

In D7.4 our enhanced opto-electrical simulations, now incorporating mobile ion effects, reveal key performance influencers in perovskite/silicon tandem solar cells. In addition, we quantified the impact of C60 interface recombination (-7.6% efficiency loss per decade of increase), C60 thickness (-0.05% efficiency loss per nm increase), and perovskite ion concentration (-1.6% efficiency loss per decade of increase). Furthermore, simulations predict a ~4% absolute efficiency gain/loss under standard test conditions when incorporating/avoiding a tailored refractive index matching layer ($n \approx 2.9$), compared to a non-ideal refractive index jump between the recombination layer (ITO) and the a-Si layers below. To broaden applicability, future model development will address non-STC scenarios, including varying illumination angles, temperatures, and spectral distributions. Temperature dependencies present a significant challenge due to their complex effects on material properties, requiring advanced optimization strategies and rigorous experimental validation, which presents a change to establish community-wide simulation standards.

This project has received funding from the European Union’s Horizon 2020 research and innovation programme under grant agreement N°101006715

1. DESCRIPTION OF SIMULATION TOOLS AND OPTIMIZATION ALGORITHM

Analogous to the previous report, D7.1, COMSOL[1], SILVACO[2] and SENTAURUS TCAD[3], as well as SETFOS[4] and the less powerful SCAPS-1D[5] are available within the consortium. Notably, an important feature previously not considered is the ability to model a secondary set of mobile charges (mobile ions) with vastly different mobilities compared to electrons and holes (ca. 7 orders of magnitude difference). This is important since previous simulations could not emulate the scenario with them present. With ever-growing focus on mobile ions, a halide-perovskite-specific property (in the context of a material used for photovoltaics), this crucial aspect cannot be neglected in the quantitative description of the cells. The considerably slower ions (relative to electrons and holes) come however at the cost of drastically longer computational times to ensure stationary conditions, i.e., simulate steady-state behaviour. With organic semiconductors surrounding the halide perovskites in most scenarios and them often forming loosely bound networks, ions may also penetrate the organic semiconductors, a currently overlooked phenomenon. Capturing such effects however poses a new set of questions, particularly related to the ion transport across interfaces. Likewise, even the above-described, most advanced, simulation tools currently available, do not capture the scenario of local cation / anion / vacancy generation or annihilation and how these effects affect the photovoltaic performance. Having such effects implemented would greatly improve the capability to model the scenario of these cells degrading in operation.

2. OPTIMIZATION ALGORITHMS REVISITED

Large multi-dimensional parameter spaces, such as is the case in multijunction solar cells, cannot be screened within reasonable timescales resulting in the need to adopt e.g., machine-learning backed methods to efficiently navigate the large parameter spaces. In the example of a perovskite-silicon tandem device a parameter space with ~15 dimensions, considering only the thicknesses of all the layers in the stack, a rough parameter screening with 5 possible settings per layer already results in $5^{15} \approx$ 30 billion combinations. With simulation durations on the order of seconds (larger clusters) to minutes (standard multithread-compatible laptop), this corresponds to 1000s of years of computation. In the previous report we outlined the efficacy of Bayesian optimization to elegantly navigate this parameter space within a few hours. Yet even this approach is speed limited by design and scales – depending on the assumptions and choice of acquisition function – roughly with $O(N^3)$ ($N =$ existing data points). For small numbers of evaluations this cubic scaling behaviour is small compared to the evaluation, yet for larger datasets, can easily outcompete the actual

This project has received funding from the European Union's Horizon 2020 research and innovation programme under grant agreement N°101006715

evaluation, thus adding to the computational cost. The problems we looked at so far, are comparably fast to compute, so that this issue does not impact us directly. In an attempt to showcase, when the modelling duration becomes relevant compared to the evaluation we showcase the exact same tandem solar cell stack, but account for field-relevant parameters by considering real-world data, including the two angles of illumination, direct and indirect illumination, the variance in the spectral distribution of the sun's light throughout the day and the season and the surrounding and device temperature (they differ, e.g., because of rain, snow or wind). A model dataset collected by colleagues from Sandia Nation Laboratories, US,[6] provides a full year's dataset including all mentioned parameters for the year 2020 with a climate not to dissimilar to the sunniest regions in Europe, e.g., southern Spain (cf. Sevilla with a frostier winter). Taking these factors into account the computational problem grows, especially in view of expanding beyond sheer optical parameters – primary focus of the previous report - since all the layers have varying, partially diverging thermal coefficients of their physical properties (bandgap, carrier mobilities, ion mobilities, effective doping, thermally activated traps, light-induced doping). In such a scenario the so-called "curse of dimensionality" becomes highly relevant.

There are, however, methods that allow to reduce the problem and reparametrize the system to a series of 1D problems[7]. In this scenario the computational time does not increase with the number of iterations (**Errore. L'origine riferimento non è stata trovata.**a) and navigates even enormous parameter spaces (e.g., 200-dimensional Ackley function with a singular minimum at 0) relatively quickly (**Errore. L'origine riferimento non è stata trovata.**b). To showcase the elegance and speed of this approach we applied it to the same problem discussed previously – a 14-dimensional thickness optimization of a perovskite-silicon tandem device. The algorithm navigates faster and detects higher overall values than the current-best Bayesian optimizer we applied at only a fraction of the time (ca 1/3, **Errore. L'origine riferimento non è stata trovata.**c). This goes to show the elegance of additional

These accelerated optimizations allow rapid optimizations of tandem devices to best perform under any given condition, e.g., when in outdoor conditions for extended periods of times. Prior to optimizing the performance of a realistic device simulation, key performance limitations must be identified and addressed to generate the best-possible starting conditions for any optimization problem.

This project has received funding from the European Union's Horizon 2020 research and innovation programme under grant agreement N°101006715

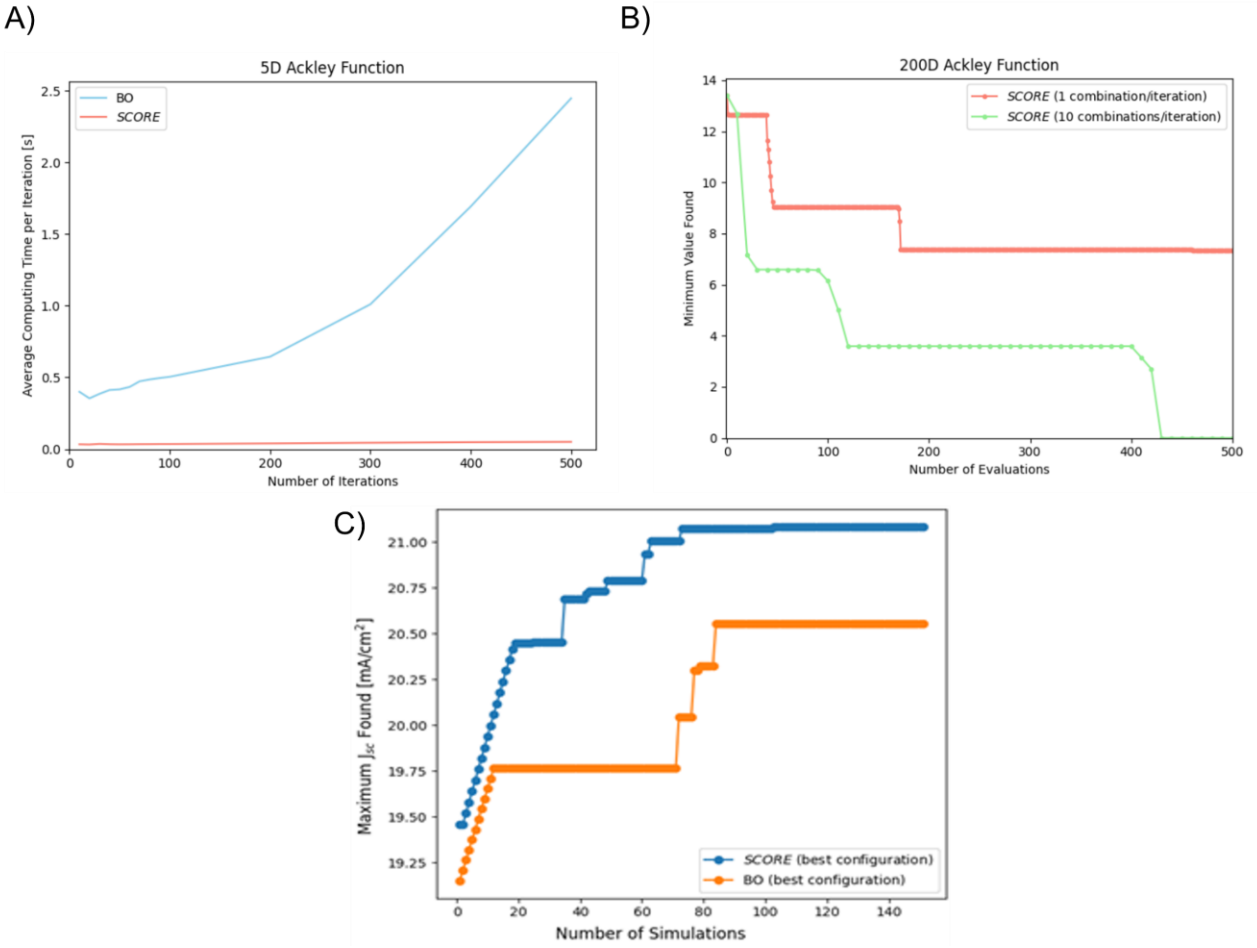

Figure 1 – A) comparison of evaluation time of a Bayesian optimization (BO) vs. the linear parametrized SCORE algorithm whose computational time is constant. B) performance of SCORE in a 200-dimensional Ackley function space for different evaluation size sets (1 vs. 10). C) performance of SCORE versus a tweaked version of BO in finding optimal thicknesses of all layers in a perovskite/silicon tandem device (14 dimensions). Panel A) and B) reproduced with permission.[7,8]

3. OVERVIEW OF KEY MATERIAL PROPERTIES AND PARAMETERS FOR OPTIMAL PERFORMANCE OF PK/Si TANDEM SOLAR CELLS

3.1 Perovskite/C60 interface region

For the given layer stack of a perovskite-silicon tandem solar cell (Figure 2c) many of the critical parameters from the single-junction devices can be directly translated, however, in some cases the

This project has received funding from the European Union's Horizon 2020 research and innovation programme under grant agreement N°101006715

relevance of some of the layers becomes diminished (e.g., parasitic absorption of a-Si:H(n) layers since perovskite absorbs that part of the light). One such example and a critical region in a perovskite/silicon tandem device is the region near the electron-transporting material C60 in the perovskite top cell. Due to its non-negligible absorption in the blue and green part of the spectrum, a thick C60 layer effectively steals light from the top-cell. This loss can be estimated directly by fitting the simulated PCE as a function of C60 thickness, rendering a loss of -0.05%/nm under standard testing conditions.

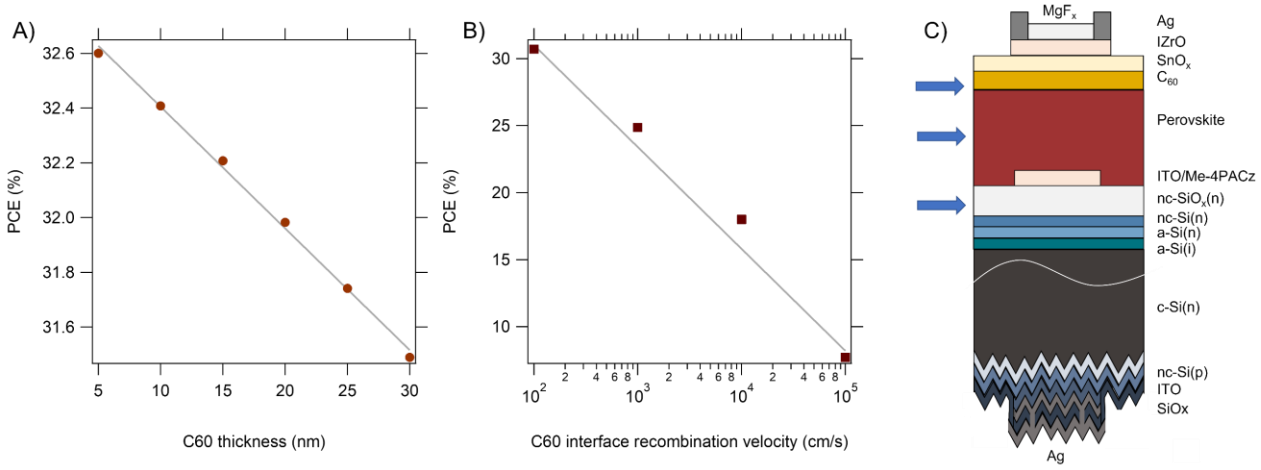

Figure 2 – A) Tandem performance for an optimized current-matched (5nm case) tandem solar cell[9] as a function of C60 layer thickness. B) Tandem performance for a standard current-matched tandem cell[10] as a function of the effective surface recombination velocity at the perovskite/C60 interface. C) Schematic of the device from B) highlighting the three newly discovered critical material property areas (four properties) with blue arrows.

Even more critical than the optical loss is the electronic loss. C60 is known to cause significant recombination losses in wider bandgap perovskite solar cells[11,12]

And so, it is no surprise that the recombination velocity at the perovskite/c60 interface is a critical parameter for the performance. Analogous to above the loss can be estimated in terms of the velocity where we estimate -7.6%/decade of recombination velocity. Currently the best-performing wide bandgap perovskites have velocities on the order of 50-100 cm/s [13], with clear pathways to reduce the latter by adequate interface passivation[14].

3.2 NIR reflection minimization through nc-SiOx (n)

In addition to electrical performances, optical performance is critical, and the refractive indices must be selected such that there are no abrupt changes, as these would result in significant reflection losses. Excluding the thin ITO layer at the recombination junction the layer stack in this region for a

This project has received funding from the European Union's Horizon 2020 research and innovation programme under grant agreement N°101006715

standard device would have a sequence of: …/perovskite/ITO/a-Si(n)/a-Si(i)/c-Si/… and a change in the mean refractive indices in the NIR region (800-1000nm) to from 2.6 (perovskite) to 4 (a-Si) and 3.6 (c-Si). Since the perovskite/ITO jump (n ~ 2.6 to n~2) cannot be replaced easily the loss stemming therefrom must be accepted, yet it's implications can be minimized by devising an interlayer behind the ITO that can minimize the reflection at this lossy interface (ITO/a-Si n~2 to n~4) with a refractive index between that of ITO and a-Si. To this end nc-SiOx with a varying oxygen content can be tuned to render both a variable refractive index between 2.4 and ~3 while balancing the resistive losses upon doping[15].

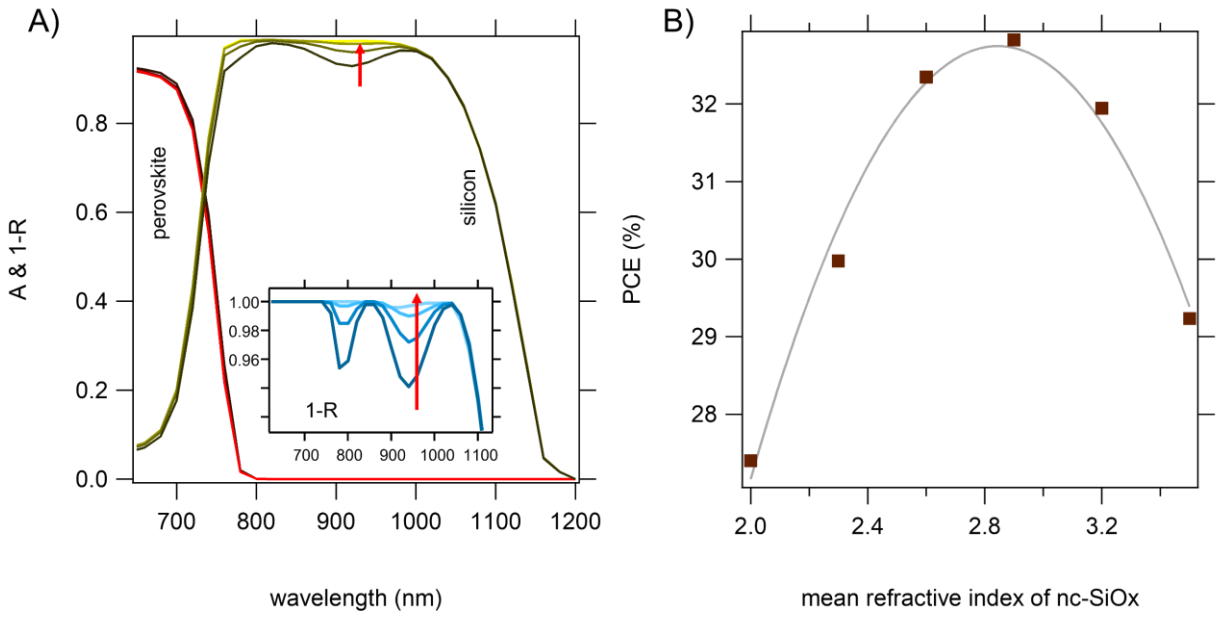

Figure 3- A) Simulated absorption (A) and reflection (1-R, inset) of perovskite-silicon tandem devices with varying effective refractive index of nc-SiOx. B) performance as a function of the mean refractive index in a matched (for n= 2.9) device.

We simulate this by varying the refractive index of such an interlayer in a stack …/perovskite/ITO/nc-SiOx/a-Si(n)/a-Si(i)/c-Si/… and visualize the effect by showing the absorptance in the c-Si and the reflection (shown as 1-R) in Figure 3a. The effect is significant, resulting in absolute performance losses more than 4% absolute when comparing n= 2 to an optimized n=2.9 case. This points to the criticality of advanced light management.

3.3 Ions in halide perovskite top cell

Halide perovskites are among the few material systems that show both electronic and ionic mobility, which was discovered early in their development through the observation of "anomalous" hysteresis[16] when comparing the forward and backward JV scan, which is history and scan-rate

This project has received funding from the European Union's Horizon 2020 research and innovation programme under grant agreement N°101006715

dependent. Only in the last few years the effect of these mobile ions has been better understood, and recently also how the generation and accumulation of mobile ions during operation impacts the apparent stabilized PCE and the stability[17]. Importantly, this also critically impacts the way different laboratories quantify the efficiency[18], when looking at complementary measurements, e.g., EQE/ spectral response compared to JV scans. One of the metastudies based on the perovskite database revealed a systematic discrepancy between the current density measured under JV scanning and EQE measurements[19].

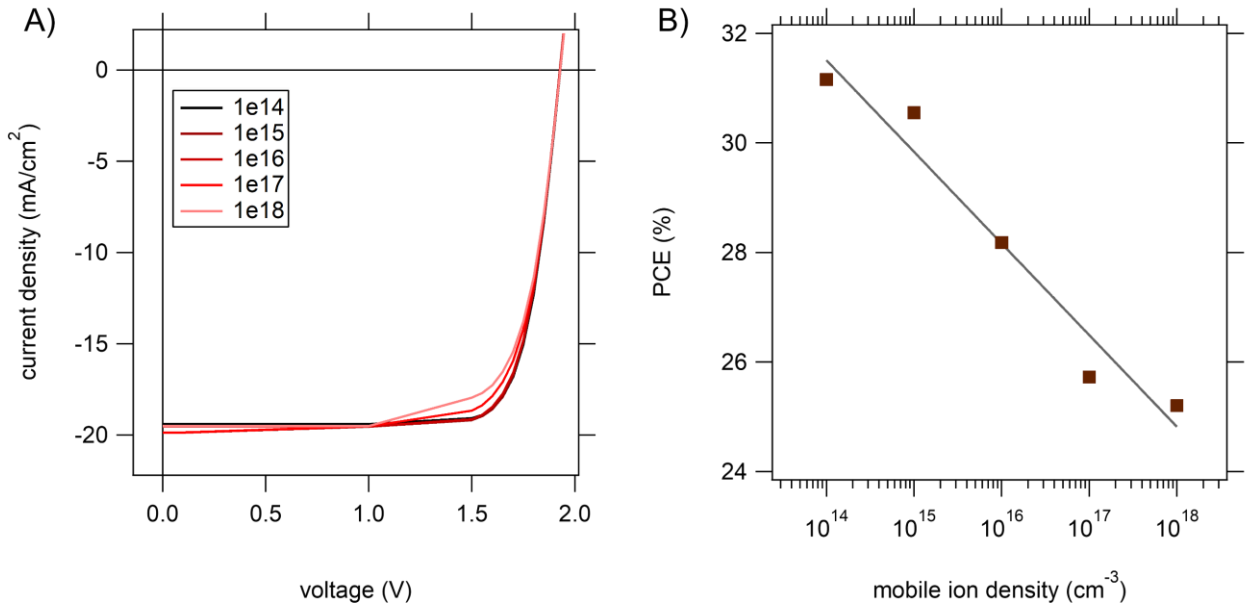

Figure 4 – A) JV curves of tandem devices featuring different balanced cation and anion densities as indicated in the legend. B) associated PCE indicating a loss that scales in first order with -1.6%/ decade of mobile ion density in the perovskite absorber.

These observations naturally translate into perovskite-silicon tandem solar cells, where the intricacy of series connects a cell that exhibits ionic movement with another one that doesn't complicate the analysis and the simulations. Even without considering lateral effects[20] – which are accentuated in small lab-scale devices - the effect of an increased ion concentration can be simulated. Starting from a standard simulation we systematically increase the mobile ion density and observe a loss of -1.6%/decade of the concentration within the range of 10^{14}-10^{18} cm^{-3}. Further simulations with concentrations below 10^{14} cm^{-3} show no effect, because there the screening potential is diminished. As a rule of thumb, reducing the ion density to below the charge carrier density will result in a saturation of any effect. With a carrier concentration of 10^{14}-10^{15} cm^{-3} under normal operation (AM1.5G)[21] this naturally sets a limit below which ionic effects are negligible. Such estimations also point towards predicting the possible impact of "just" increasing the ionic density as a function of time

This project has received funding from the European Union's Horizon 2020 research and innovation programme under grant agreement N°101006715

in operation, even without terminal chemical degradation due to redox reactions, which can be possibly avoided by careful selection of the layers.

3.4 Overview of critical layers and parameters

To summarize the findings and additional new findings, the previously reported table is augmented with new entries to capture the above-discussed new insights. The sensitivity is marked with +++ = strong to - = irrelevant to indicate the relevance to performance.

Material	Relevant Properties	Sensitivity	Comments
Top Ag	Resistivity	+	the contact resistance to IZO is impacted by the fabrication and the layer thickness impacts the overall resistance of the device, has to be optimized for the respective design
MgF2	Layer thickness	++	Enables modulation of reflection into the device (cf. quarter wavelength rule)
IZO	Thickness	+	The carrier density, mobility and thickness of this layer impacts the optical performance (parasitic absorption in the UV and IR through free-carrier absorption). This must be optimized versus the optimal lateral conductivity to enable efficient transport and can be partially palliated through a smart top Ag grid design
	Doping density / mobility	+	
SnO2	Thickness / conductivity	-	Within the typical thickness range of SnO_2 (10-50 nm) the typically grown SnO_2 layers with mobilities > 10cm^2/Vs and small doping densities < $10^{17}cm^{-3}$ have a negligible impact on the device performance
C60	Thickness / conductivity	+	C_{60} absorbs a substantial portion of the UV-green light and has a comparably low electron mobility (0.2 cm^2/Vs in the best case) rendering it necessary to reduce the thickness of this layer as much as possible, the loss rate here corresponds to ca. -0.05% / nm. Likewise, the recombination at this interface is critical, where the loss is estimated to scale with 7.6%/decade of the interface recombination velocity. Typical values currently lie around 50-100cm/s for wide bandgap perovskites and as low as 10 for lower bandgap perovskites.
	Interface recombination velocity	+++	

This project has received funding from the European Union's Horizon 2020 research and innovation programme under grant agreement N°101006715

Perovskite	Bandgap/ thickness	++	The thickness and bandgap of the perovskite are pivotal in determining the performance of a tandem device. For optimal performance the bandgap should be maximized while assuring sufficient thickness for optimal absorption. For too low carrier mobilities the generated carriers can however not reach the contacts and are lost. Similarly, a high defect density would negatively impact the produced photovoltage and transport resulting in low performance. Accordingly, these four parameters must be taken into consideration in concert for optimal performance. Especially considering that additionally mobile ions impact the transport of photogenerated charges by counteracting the electric field in the device under steady-state conditions. The ion concentration has a measurable loss with a predicted -1.6%/decade of ion concentration.
	Mobility	++	
	Defect density	++	
	Ionic density	+++	
ITO	Doping density	+	The typically thin layers for the recombination junction are also lowly doped, to limit parasitic absorption in the IR, yet there is only a weak sensitivity
nc-SiOx	refractive index	+++	Optimal light-in-coupling into the Si bottom solar cell the requires minimal change in the refractive indices in the relevant range (~800-1200 nm) and the material must be selected carefully. Doped SiOx offers a wide tunability through the doping density and the stoichiometry, where higher oxygen contents result in lower refractive index, but also lower conductivity. Balancing optical and electrical performance in this layer is critical.
a-Si:n	Thickness	+	Despite the typically low thickness, these layers can cause significant optical losses upon too high doping or high thickness. Fortunately, the perovskite layer allows for more relaxed conditions w.r.t. thickness (compared to single junctions), since it absorbs most of the light the a-Si would otherwise absorb.
	Doping density	++	
a-Si:i	Thickness	+	The low mobility in these layers requires them to be thin to limit resistive and optical losses
c-Si	Doping density/thickness	+	Industry-grade silicon wafers with low resistivity are of sufficient quality to allow for efficient absorption and transport within a wide range of thicknesses (100-300um), notably the

This project has received funding from the European Union's Horizon 2020 research and innovation programme under grant agreement N°101006715

			thickness impacts the efficiency of the devices through a modification of the current matching conditions
a-Si:i	Thickness	+	The low mobility in these layers requires them to be thin to limit resistive and losses
a-Si:p	Doping density	++	Despite the typically low thickness, these layers can cause significant optical losses (reflection upon double pass) upon too high doping
	Thickness	++	
ITO	Doping density	-	The rear-side ITO is typically lowly doped and reasonably thin to separate the Ag from the a-Si and reduce resistive and electrical losses with little impact
	Thickness	-	
Bottom Ag	Thickness	+/-	the contact resistance to ITO is impacted by the fabrication and the layer thickness impacts the overall resistance of the device, must be optimized for the respective design

4. CONCLUSIONS & OUTLOOK

In this report additional new opto-electrical simulations featuring refined models and including mobile ions are presented. Beyond the already discussed key material properties four particularly important materials/layers/properties have been newly discussed in greater detail featuring a more in-depth analysis and quantification of their impact on performance under standard test conditions. These are: C60 interface recombination velocity (-7.6% / decade), C60 thickness (-0.05% / nm), perovskite ion concentration (-1.6% / decade) as well as the possibility of introducing a refractive bridge layer (e.g., nano-crystalline n-doped SiOx) with a tailored refractive index (ca. 2.9) to reduce reflective losses in the silicon bottom cell. Depending on the current matching scenario a loss ~ 4% absolute (e.g., material with n=2.0 vs n=2.9) is to be expected. It is important to note that all the previous and current simulations are carried out based on standard test conditions (assuming 25°C and direct illumination at 90° incidence angle). To better predict and assist in future application scenarios, within future projects, the datasets need to be adapted to account for varying illumination angles (azimuthal, zenith), temperatures, varying spectra and partial diffuse and albedo illumination. In particular temperature adds complexity as all the optoelectrical properties may exhibit strong temperature dependencies that are non-trivial to model, with the examples shown in Figure 5 (diverging bandgap shifts, mobility depending on transport type, etc.). As such the halide perovskites exhibit a bandgap narrowing for higher temperatures, while c-Si with its' indirect bandgap shows the opposing trend (Figure 5A). On the other hand, also the electronic properties are impacted.

This project has received funding from the European Union's Horizon 2020 research and innovation programme under grant agreement N°101006715

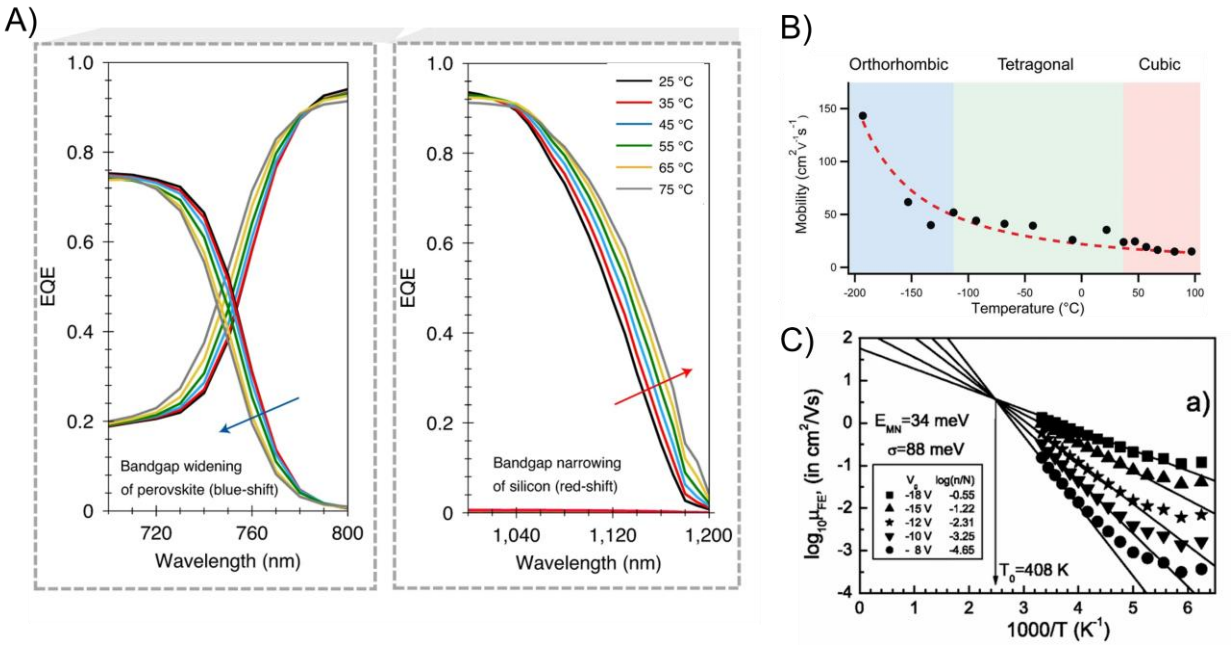

Figure 5 – A) Bandgap shift of perovskite and silicon tandem device for increasing temperature. B) mobility (extracted via THz spectroscopy) of a $MAPbI_3$ perovskite as a function of temperature together with a fit line ($T^{-3/2}$ as expected for band transport). C) electron mobility of C60 as a function of temperature and bias in an FET configuration, increasing with temperature, as expected, for a material exhibiting hopping transport. Reproduced with permission (A[22],B[23] ,C[24]).

For example, the mobility in materials with band transport is typically reduced when increasing the temperature due to a higher likelihood of electron-phonon scattering (Figure 5b), while for organic transport layers such as C60 transport is improved (Figure 5c). This may be the cause for the small temperature coefficient of perovskite single junctions but is hardly understood in tandem devices. All these considerations add complexity and thus requires re-thinking methods to optimize simulations with algorithms even faster than the discussed Bayesian optimization and possibly the reparameterization outlined above (cf. SCORE), will enable faster. It is furthermore non-trivial to compare different simulation tools which, a priory, are based on the same physics and the equations describing them. This is particularly relevant for interfaces and therefor by extension for multijunction devices, that contain many more interfaces than single-junction cells. An example here is the description of the recombination junction, where electrons from one cell recombine with holes from the other cell, e.g., via trap-assisted recombination, tunnelling, or similar. We believe that these complications are in-fact chances! They enable to establish new standards in the field of solar energy device modelling and deserve concerted efforts to allow for improved, standardized models validated through experiments, which in turn will accelerate the experimental realization of even better performing multijunction devices, including perovskite/silicon tandems as discussed herein.

This project has received funding from the European Union's Horizon 2020 research and innovation programme under grant agreement N°101006715

5. BIBLIOGRAPHY

(1) Jacobs, D. A.; Wu, Y.; Shen, H.; Barugkin, C.; Beck, F. J.; White, T. P.; Weber, K.; Catchpole, K. R. Hysteresis Phenomena in Perovskite Solar Cells: The Many and Varied Effects of Ionic Accumulation. *Physical Chemistry Chemical Physics* **2017**, *19* (4), 3094–3103. https://doi.org/10.1039/C6CP06989D.

(2) Boukortt, N. E. I.; Patanè, S.; AlAmri, A. M.; AlAjmi, D.; Bulayyan, K.; AlMutairi, N. Numerical Investigation of Perovskite and U-CIGS Based Tandem Solar Cells Using Silvaco TCAD Simulation. *Silicon* **2023**, *15* (1), 293–303. https://doi.org/10.1007/s12633-022-01960-9.

(3) Restat, L.; Messmer, C.; Heydarian, M.; Heydarian, M.; Schoen, J.; Schubert, M. C.; Glunz, S. W. Optoelectrical Modeling of Perovskite/Perovskite/Silicon Triple-Junction Solar Cells: Toward the Practical Efficiency Potential. *Solar RRL* **2024**, *8* (5), 2300887. https://doi.org/10.1002/SOLR.202300887.

(4) Thiesbrummel, J.; Shah, S.; Gutierrez-Partida, E.; Zu, F.; Peña-Camargo, F.; Zeiske, S.; Diekmann, J.; Ye, F.; Peters, K. P.; Brinkmann, K. O.; Caprioglio, P.; Dasgupta, A.; Seo, S.; Adeleye, F. A.; Warby, J.; Jeangros, Q.; Lang, F.; Zhang, S.; Albrecht, S.; Riedl, T.; Armin, A.; Neher, D.; Koch, N.; Wu, Y.; Le Corre, V. M.; Snaith, H.; Stolterfoht, M. Ion-Induced Field Screening as a Dominant Factor in Perovskite Solar Cell Operational Stability. *Nat Energy* **2024**. https://doi.org/10.1038/s41560-024-01487-w.

(5) Burgelman, M.; Nollet, P.; Degrave, S. Modelling Polycrystalline Semiconductor Solar Cells. *Thin Solid Films* **2000**, *361–362*, 527–532. https://doi.org/10.1016/S0040-6090(99)00825-1.

(6) Driesse, A.; Stein, J. *Global Normal Spectral Irradiance in Albuquerque: A One-Year Open Dataset for PV Research*; Albuquerque, NM, and Livermore, CA (United States), 2020. https://doi.org/10.2172/1814068.

(7) Chakar, J. SCORE: A 1D Reparameterization Technique to Break Bayesian Optimization's Curse of Dimensionality. **2024**.

(8) Chakar, J.; Anand, S.; Wolff, C. M.; Puel, J.-B.; Bonnasieux, Y. Advanced Optical Optimization of Tandem and Triple-Junction Solar Cells. *submitted*.

(9) Chin, X. Y.; Turkay, D.; Steele, J. A.; Tabean, S.; Eswara, S.; Mensi, M.; Fiala, P.; Wolff, C. M.; Paracchino, A.; Artuk, K.; Jacobs, D.; Guesnay, Q.; Sahli, F.; Andreatta, G.; Boccard, M.; Jeangros, Q.; Ballif, C. Interface Passivation for 31.25%-Efficient Perovskite/Silicon Tandem Solar Cells. *Science (1979)* **2023**, *381* (6653), 59–63. https://doi.org/10.1126/science.adg0091.

This project has received funding from the European Union's Horizon 2020 research and innovation programme under grant agreement N°101006715

(10) Turkay, D.; Artuk, K.; Chin, X.-Y.; Jacobs, D. A.; Moon, S.-J.; Walter, A.; Mensi, M.; Andreatta, G.; Blondiaux, N.; Lai, H.; Fu, F.; Boccard, M.; Jeangros, Q.; Wolff, C. M.; Ballif, C. Synergetic Substrate and Additive Engineering for over 30%-Efficient Perovskite-Si Tandem Solar Cells. *Joule* **2024**, *8* (6), 1735–1753. https://doi.org/10.1016/j.joule.2024.04.015.

(11) Warby, J.; Zu, F.; Zeiske, S.; Gutierrez-Partida, E.; Frohloff, L.; Kahmann, S.; Frohna, K.; Mosconi, E.; Radicchi, E.; Lang, F.; Shah, S.; Peña-Camargo, F.; Hempel, H.; Unold, T.; Koch, N.; Armin, A.; De Angelis, F.; Stranks, S. D.; Neher, D.; Stolterfoht, M. Understanding Performance Limiting Interfacial Recombination in Pin Perovskite Solar Cells. *Adv Energy Mater* **2022**, *12* (12), 2103567. https://doi.org/10.1002/aenm.202103567.

(12) Suchan, K.; Jacobsson, J.; Rehermann, C.; Simmonds, M.; Unger, E.; Kirchartz, T.; Wolff, C. M. Rationalizing Performance Losses of Wide Bandgap Perovskite Solar Cells Evident in Data from the Perovskite Database. *Adv Energy Mater* **2023**, *in prep.*

(13) Stolterfoht, M.; Wolff, C. M.; Márquez, J. A.; Zhang, S.; Hages, C. J.; Rothhardt, D.; Albrecht, S.; Burn, P. L.; Meredith, P.; Unold, T.; Neher, D. Visualization and Suppression of Interfacial Recombination for High-Efficiency Large-Area Pin Perovskite Solar Cells. *Nat Energy* **2018**, *3* (10), 847–854. https://doi.org/10.1038/s41560-018-0219-8.

(14) Liu, J.; Bastiani, M.; Aydin, E.; Harrison, G. T.; Gao, Y.; Pradhan, R. R.; Eswaran, M. K.; Mandal, M.; Yan, W.; Seitkhan, A.; Babics, M.; Subbiah, A. S.; Ugur, E.; Xu, F.; Xu, L.; Wang, M.; Rehman, A. U.; Razzaq, A.; Kang, J.; Azmi, R.; Said, A. A.; Isikgor, F. H.; Allen, T. G.; Andrienko, D.; Schwingenschlögl, U.; Laquai, F.; Wolf, S. Efficient and Stable Perovskite-Silicon Tandem Solar Cells through Contact Displacement by MgFx. *Science* **2022**, *377* (6603), 302–306. https://doi.org/10.1126/science.abn8910.

(15) Cruz, A.; Erfurt, D.; Wagner, P.; Morales-Vilches, A. B.; Ruske, F.; Schlatmann, R.; Stannowski, B. Optoelectrical Analysis of TCO+Silicon Oxide Double Layers at the Front and Rear Side of Silicon Heterojunction Solar Cells. *Solar Energy Materials and Solar Cells* **2022**, *236*, 111493. https://doi.org/10.1016/j.solmat.2021.111493.

(16) Snaith, H. J.; Abate, A.; Ball, J. M.; Eperon, G. E.; Leijtens, T.; Noel, N. K.; Stranks, S. D.; Wang, J. T.-W. W.; Wojciechowski, K.; Zhang, W. Anomalous Hysteresis in Perovskite Solar Cells. *Journal of Physical Chemistry Letters* **2014**, *5* (9), 1511–1515. https://doi.org/10.1021/jz500113x.

(17) Thiesbrummel, J.; Shah, S.; Gutierrez-Partida, E.; Zu, F.; Peña-Camargo, F.; Zeiske, S.; Diekmann, J.; Ye, F.; Peters, K. P.; Brinkmann, K. O.; Caprioglio, P.; Dasgupta, A.; Seo, S.; Adeleye, F. A.; Warby, J.; Jeangros, Q.; Lang, F.; Zhang, S.; Albrecht, S.; Riedl, T.; Armin, A.; Neher, D.; Koch, N.; Wu, Y.; Le Corre, V. M.; Snaith, H.; Stolterfoht, M. Ion-Induced Field Screening as a Dominant Factor in Perovskite Solar

This project has received funding from the European Union's Horizon 2020 research and innovation programme under grant agreement N°101006715

Cell Operational Stability. *Nature Energy 2024 9:6* **2024**, *9* (6), 664–676. https://doi.org/10.1038/s41560-024-01487-w.

(18) Messmer, C.; Chojniak, D.; Bett, A. J.; Reichmuth, S. K.; Hohl-Ebinger, J.; Bivour, M.; Hermle, M.; Schön, J.; Schubert, M. C.; Glunz, S. W. Toward More Reliable Measurement Procedures of Perovskite-Silicon Tandem Solar Cells: The Role of Transient Device Effects and Measurement Conditions. *Progress in Photovoltaics: Research and Applications* **2024**. https://doi.org/10.1002/pip.3782.

(19) Saliba, M.; Unger, E.; Etgar, L.; Luo, J.; Jacobsson, T. J. A Systematic Discrepancy between the Short Circuit Current and the Integrated Quantum Efficiency in Perovskite Solar Cells. *Nature Communications 2023 14:1* **2023**, *14* (1), 1–6. https://doi.org/10.1038/s41467-023-41263-0.

(20) Jacobs, D. A.; Wolff, C. M.; Chin, X.-Y.; Artuk, K.; Ballif, C.; Jeangros, Q. Lateral Ion Migration Accelerates Degradation in Halide Perovskite Devices. *Energy Environ Sci* **2022**, *15* (12), 5324–5339. https://doi.org/10.1039/D2EE02330J.

(21) Wolff, C. M.; Bourelle, S. A.; Phuong, L. Q.; Kurpiers, J.; Feldmann, S.; Caprioglio, P.; Marquez, J. A.; Wolansky, J.; Unold, T.; Stolterfoht, M.; Shoaee, S.; Deschler, F.; Neher, D. Orders of Recombination in Complete Perovskite Solar Cells – Linking Time-Resolved and Steady-State Measurements. *Adv Energy Mater* **2021**, *11* (45), 2101823. https://doi.org/10.1002/aenm.202101823.

(22) Aydin, E.; Allen, T. G.; De Bastiani, M.; Xu, L.; Ávila, J.; Salvador, M.; Van Kerschaver, E.; De Wolf, S. Interplay between Temperature and Bandgap Energies on the Outdoor Performance of Perovskite/Silicon Tandem Solar Cells. *Nature Energy 2020 5:11* **2020**, *5* (11), 851–859. https://doi.org/10.1038/s41560-020-00687-4.

(23) Milot, R. L.; Eperon, G. E.; Snaith, H. J.; Johnston, M. B.; Herz, L. M. Temperature-Dependent Charge-Carrier Dynamics in CH3NH3PbI3 Perovskite Thin Films. *Adv Funct Mater* **2015**, *25* (39), 6218–6227. https://doi.org/10.1002/ADFM.201502340.

(24) Fishchuk, I. I.; Kadashchuk, A. K.; Genoe, J.; Ullah, M.; Sitter, H.; Singh, Th. B.; Sariciftci, N. S.; Bässler, H. Temperature Dependence of the Charge Carrier Mobility in Disordered Organic Semiconductors at Large Carrier Concentrations. *Phys Rev B* **2010**, *81* (4), 1–12. https://doi.org/10.1103/PhysRevB.81.045202.

This project has received funding from the European Union's Horizon 2020 research and innovation programme under grant agreement N°101006715